Carbon-resistant NiO-Y_2O_3-nanostructured catalysts derived from double-layered hydroxides for dry reforming of methane

Katarzyna Świrk [1,2,*,a,b], Hailong Zhang [1], Shanshan Li [3], Yaoqiang Chen [4], Magnus Rønning [5], Monika Motak [2], Teresa Grzybek [2], Patrick Da Costa [1]

[1] Sorbonne Université, Institut Jean Le Rond d'Alembert, CNRS UMR 7190, Saint-Cyr-l'Ecole F-78210, France

[2] AGH University of Science and Technology, Faculty of Energy and Fuels, Cracow 30-059, Poland

[3] State Key Laboratory of Polymer Materials Engineering of China (Sichuan University), Polymer Research Institute of Sichuan University, Chengdu 610065, China

[4] College of Chemistry, Sichuan University, Chengdu 610064, China

[5] Norwegian University of Science and Technology, Department of Chemical Engineering, Trondheim N-7491, Norway

[a] Current address: Institut Charles Gerhardt Montpellier, Université de Montpellier, DAMP, CNRS UMR 5253, Place Eugène Bataillon, 34095, Montpellier, Cedex 5, France.

[b] Current address: Institut Charles Gerhardt Montpellier, Université de Montpellier, Ecole Nationale Supérieure de Chimie de Montpellier, MACS, CNRS UMR 5253, 240 Avenue du Professeur Emile Jeanbrau, 34296, Montpellier, Cedex 5, France.

Keywords: Nickel, Yttrium Oxide, Dry Methane Reforming, Carbon Resistance

Corresponding author: Katarzyna Świrk, katarzyna.swirk@sorbonne-universite.fr

Abstract

Yttrium promoted Ni/Mg/Al double-layered hydroxides were prepared through co-precipitation method and calcined at 550 °C for 5 h in order to obtain nanostructured mixed oxides. The catalysts were tested in dry reforming of methane (DRM) at 700 °C for 5 h, and characterized by X-ray diffraction, N_2 adsorption-desorption, X-ray fluorescence, temperature programmed reduction in H_2, temperature programmed desorption of CO_2, thermogravimetric analysis, Raman spectroscopy, high-resolution transmission electron microscopy, and EDS elemental mapping carried out through transmission electron microscopy. It was found that with the increasing Y content the reducibility of Ni species and total basicity increased. Yttrium promotion with assumed 3.0 and 4.0 wt.% resulted in higher CH_4 and CO_2 conversions and H_2/CO molar ratio compared to unmodified catalyst. However, the samples suffered from the significant amount of carbon deposits. The best catalytic stability was found for NiY8-DLH (presumed Y of 8.0 wt.%), being highly resistant to coke formation in DRM.

1. Introduction

The clear need for the development of sustainable valorization of the energy sources has drawn tremendous attention. Hydrogen and carbon monoxide are promising emerging candidates. A mixture of these two gases is known as synthesis gas, and one of the reactions which deals with its production is dry reforming of methane (DRM) [1]. In this reaction, the produced ratio between H_2/CO is appropriate for products including Fischer-Tropsch fuels (process on Fe-based catalysts) and dimethyl ether (DME) [2]. In comparison to conventional technologies, i.e., steam reforming and partial oxidation of methane, the DRM is also suitable for remote natural gas or crude oil fields, where water supplies are limited [3]. Moreover, since natural gas deposits include large amounts of CO_2, its emission to the atmosphere can be avoided if carbon dioxide was used in DRM. This would lower the purification costs [4]. The particular

conditions needed for practical industrial application of DRM are directly linked to its thermodynamic and kinetic barriers, as well as lack of a proper catalyst [5].

Many studies have reported the application of various types of catalysts for the dry reforming of methane. Supported noble metals (Rh, Ru, Pt, Pd, Ir) show excellent catalytic performance with almost no carbon deposition. However, their limited availability and high cost hinder their industrial application. A low-cost alternative may be non-noble metals, such as Ni or Co. Despite good catalytic properties of cobalt its application is critically and strategically restricted since cobalt has a high risk associated with its supply [6]. Nickel-based materials are also catalytically active in reforming of methane processes. Nevertheless, their rate of carbon formation is much higher as compared to the noble metal- and cobalt-containing materials. Formation of carbon affects stability of the used catalysts; once deposited on the surface blocks the active sites that consequently become inaccessible to the gaseous reactants. The carbon is formed upon side reactions, such as direct CH_4 decomposition and CO dis-proportionation reaction. Another problem is the sintering of the particles which play a role of active sites. The sintering is a result of exothermic reaction and/or overheating.

To prevent the deactivation of catalysts, a usage of promoters is proposed. Zhang et al. [7] studied (La, Ce, Ca, Mg)–γ-Al_2O_3 nanocomposites in dry reforming of methane. All the applied promoters contributed to more medium-strength basic sites on the catalyst surface, which could facilitate the adsorption/activation of CO_2 and the gasification of amorphous carbon, improving the catalytic properties and accelerating the coke elimination rate. The lowest amount of formed carbon deposits was observed for Ni/La_2O_3–γ-Al_2O_3. Pompeo et al. [8] reported a positive effect of Li addition on Ni/SiO_2. Introduction of 1 wt.% of lithium increased significantly the resistance to deactivation by carbon deposition. The influence of gallium on MCM-41 catalyst was studied by Al-Fatesh et al. [9]. The introduction of Ga to the catalysts decreased the number of medium and strong basic sites and reduced the amount of carbon deposited. After the DRM experiment at 800 °C, almost no carbon formation was registered for 3 %Ga + 5 %Ni/MCM-41.

Recently, the development of Ni-based catalytic supports promoted with Y has become of interest for use in the dry reforming of methane as they pose several advantages. They reveal high dispersion of nickel nanoparticles, improved textural properties, and enhanced oxygen vacancies [[10], [11], [12], [13], [14], [15], [16], [17], [18]]. All these features contribute to better resistance towards carbon deposition. In our previous studies, we showed that Y-

promoted Ni/Mg/Al-double layered hydroxides are promising catalysts for DRM [15,16]. The properties of double-layered hydroxides (DLHs), such as high surface area, good mechanical strength, abundant but moderate strength basicity, and formation of homogeneous mixtures of oxides with very small crystal size make them attractive catalyst supports for highly endothermic reactions [19]. In our previous reports yttrium loadings were in the range of 0.2–1.5 wt.% [15,16]. The Y addition led to a smaller Ni° crystallite size, a decrease in reducibility of the nickel, and a decreased number of weak and medium basic sites in the modified Ni-DLHs catalysts. It was also shown that yttrium promotion improved catalytic activity resulting in higher CH_4 and CO_2 conversions at 700 °C, with no deactivation, i.e., no decrease in catalytic activity was observed after 5 h run. However, in our studies, carbon deposits were always present. Also, yttrium species were never observed by us as a separate phase in Ni/Mg/Al double-layered hydroxides.

The aim of this study is filling the gap in research on the Y-promoted Ni/Al/Mg hydrotalcite-derived catalysts for dry reforming of methane. The effect of Y promotion with assumed loadings of 3, 4 and 8 wt.% was examined in order to understand the enhanced catalytic activity and stability in the studied catalysts.

2. Experimental

2.1. Catalysts synthesis

Double-layered hydroxides were prepared by co-precipitating an aqueous solution of nickel, magnesium and aluminum cations with a highly basic carbonate solution at 65 °C. The first solution assumed the presence of $Ni(NO_3)_2{\cdot}6H_2O$ (Sigma Aldrich, 98.5 % pure), $Mg(NO_3)_2{\cdot}6H_2O$ (Sigma Aldrich, 99 % pure), $Al(NO_3)_3{\cdot}9H_2O$ (Sigma Aldrich, 98 % pure) and $Y(NO_3)_3{\cdot}6H_2O$ (Aldrich, 99.8 % pure) in distilled water with an $M^{+3}/(M^{+2} + M^{3+})$ molar ratio of 0.25 and a Ni^{2+}/Mg^{2+} molar ratio of 0.33. Three materials were synthesized in such a way aiming at different concentrations of yttrium (3, 4 or 8 wt.%). The second (basic) solution was prepared by dissolving Na_2CO_3 in distilled water. An aqueous solution of NaOH (2 M) was added dropwise for keeping a pH of 10 ± 0.2. The Ni/Y/Mg/Al-double-layered hydroxides were filtered and dried overnight in air at 100 °C. The obtained powder was calcined at 550 °C for 5 h in a static calcination furnace.

2.2. Physico-chemical characterization

2.2.1. X-ray diffraction (XRD)

Powder X-ray diffraction patterns were recorded with an Empyrean diffractometer from PANalytical, using Cu Kα radiation (λ = 0.15418 nm) at a scanning step of 0.013°, diffraction angles 2θ = 3–90°.

2.2.2. Adsorption-desorption of nitrogen

The adsorption–desorption isotherms were measured at −196 °C by using a Micromeritics TriStar II 3020 instrument. Before the measurement, the catalyst was degassed at 110 °C for 3 h in a VacPrep 061 degasser unit.

2.2.3. X-ray fluorescence (XRF)

The chemical composition of the samples was determined by a Wavelength Dispersive X-Ray Fluorescence (WDXRF) in a Supermini200 analyzer. The sample was prepared by mixing a catalyst powder with boric acid assuming a ratio 1:40. Boric acid acted as a binder, the mixture was then pelletized under a press of 10 bars. The formed pellet was covered with polypropylene film (6 μm) and placed in the sample holder. The sample was then measured at 36.5 °C, under 24.7 ml/min of P-10 gas (10 % methane in argon).

2.2.4. Temperature programmed reduction in H_2 (TPR-H_2)

Temperature programmed reduction curves were obtained by using a BELCAT-M apparatus from BEL Japan, equipped with a thermal conductivity detector (TCD). Firstly, the catalyst (60 mg) was treated with Ar at 100 °C for 2 h, and then reduced up to 900 °C using a mixture of 5 % hydrogen in argon at a heating rate of 10 °C/min.

2.2.5. Temperature programmed desorption of CO_2 (TPD-CO_2)

The basicity of reduced catalysts was analyzed by means of temperature programmed desorption in CO_2, using a BELCAT-M apparatus. After TPR-H_2measurement, the catalyst was purified with He. The temperature was set to 80 °C, and a mixture of 10 % of carbon dioxide in helium was fed for 1 h. Subsequently, a flow of He was applied for 15 min to desorb the

physically adsorbed CO_2. Then, the catalyst was heated up under helium at 10 °C/min. The evolution of carbon dioxide desorption was analyzed with the aid of a TCD.

2.2.6. Thermogravimetric analysis (TGA)

Thermogravimetric measurements were performed in a China HCT-2 analyzer. 6 mg of the sample was used to measure weight loss. For each test, the sample was heated in air flow (45 ml/min) from room temperature up to 900 °C at a heating rate of 10 °C/min.

2.2.7. Raman spectroscopy

Raman spectra of the samples were measured in an InVia Reflex spectrometer equipped with a YAG laser (532 nm). The output power of 0.9 mW was used for Raman tests in the scanning range of 1000–3200 cm^{-1}. The spectrometer contained 600 grooves mm^{-1} of grating and a CCD detector with ×50 magnification objective lens.

2.2.8. High-resolution transmission electron microscopy (HRTEM)

HRTEM measurements were carried out on a JEOL JEM 2010 transmission electron microscope. The ethanol-based suspensions containing analyzed samples were first sonicated, and then a few drops of the suspension were deposited on copper coated carbon grids. The average size of Ni particles was calculated assuming the length of 200 particles measured in ImageJ program.

2.2.9. EDS elemental mapping through transmission electron microscopy (TEM)

EDS elemental mapping of the NiY8-DLH spent catalyst was performed in a JEM-2100 Plus transmission electron microscope. Magnesium, nickel, oxygen, yttrium and aluminum maps were obtained.

2.3. Catalytic performance in dry reforming of methane

Dry reforming of methane (DRM) experiments were performed to study the catalytic performance of the synthesized catalysts. The catalytic runs were carried out in the fixed-bed reactor at atmospheric pressure with a gas hourly space velocity (GHSV) of 20,000 h^{-1}. Before the catalytic test, the sample was reduced in situ at 900 °C for 1 h with a 5 % hydrogen in argon mixture (100 cm^3/min). Then, the mixture of $CH_4/CO_2/Ar = 1/1/8$ (10 %CH_4/10 %CO_2/80 %Ar)

was applied for 5 h at 700 °C. For heating, an electric furnace was used. The reactants (CH_4 and CO_2) and possible products (H_2, CO) were analyzed by a micro-GC (490 Varian Micro-GC).

3. Results and discussion

3.1. Structural, textural properties and elemental composition

XRD diffractograms of freshly synthesized catalysts are presented in Fig. 1. The hydrotalcite structure of $Mg_6Al_2(OH)_{16}CO_3 \cdot 4H_2O$ (ICDD 00-014-0191) with a rhombohedral symmetry (R3) was registered at 2θ of ca. 11°, 23°, 35°, corresponding to (0 0 3), (0 0 6), (0 0 9) planes, respectively. A small shift of the d_{003} and d_{006} towards lower angles was observed after promotion with 3 wt.% and 4 wt.% of yttrium. This effect was more pronounced after introduction of 8 wt.% of Y, and indicates that CO_3^{2-} was not the only anion in the interlayer regions [[20], [21], [22], [23]]. For NiY4-DLH and NiY8-DLH samples less intense and wider reflections were observed, also in case of asymmetric peaks registered at 39° and 47° arising from (0 1 5) and (0 1 8) crystal planes, respectively. This is in line with Fernández et al. [24]. The authors reported that only yttrium loading higher than 4 wt.%, could result in distortions in the DLHs layers, recognized as very low crystallinity observed in XRD patterns. Additionally, for the samples Ni-DLH and NiY3-DLH, the well-defined (1 1 0) and (1 1 3) diffractions were recorded at 60° and 61°, indicating a presence of various cations homogeneously dispersed in the hydroxide layers [25].

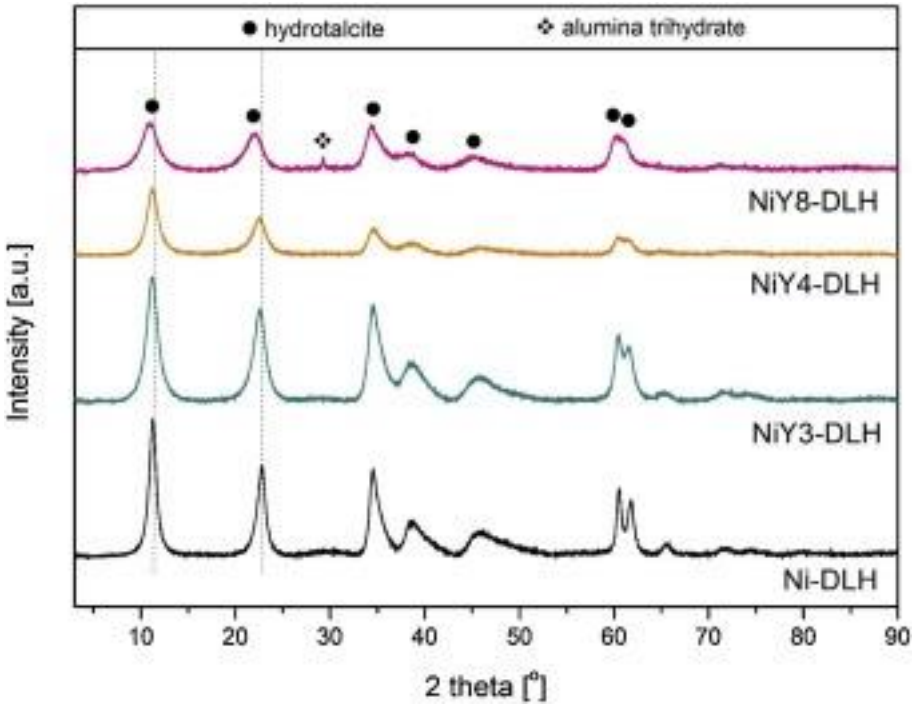

Fig. 1. XRD patterns of the freshly synthesized catalysts Ni-DLH, NiY3-DLH, NiY4-DLH, and NiY8-DLH.

Apart from reflections of hydrotalcite structure, a very weak reflection peak at 2θ of ca. 28° was registered for NiY8-DLH, indicating the existence of $Al_2O_3 \cdot 3H_2O$ phase (ICDD 00-001-0774) [26]. The values of the unit cell parameters *c* and *a*(for non-calcined materials) are shown in Table 1. The obtained values of *c*, referring to the triple distance between brucite-like layers, changed after Y-modification as compared to the non-modified material. This change was the most marked for NiY8-DLH, indicating a deposition of Y compound on the external surface. Pavel et al. [27] studied Ni-free Mg/Al hydrotalcites modified with Y (0.49 and 1.25 wt.%). For both materials the authors found an increase of *c* parameter suggesting Y aggregation on the external surface. In our study, the *c* parameter noticeably increased with Y loading confirming the existence of interlayer species, probably yttrium ones, and possibly presence of ions bigger than CO_3^{2-} [19,[21], [22], [23]]. The lattice parameter *a*, defined as the cation–cation distance in the brucite-like layers, also increased after yttrium loading of 8 wt.%. This agrees with the work of García-García et al. [28] in which it was observed that yttrium introduction into DLHs layers led to lattice distortions, i.e. changes in the lattice parameter *a*. This may be the explained by ionic radius of Y^{3+} bigger than that of Mg and Al (Y^{3+} = 1.04 Å, Mg^{3+} = 0.86 Å, Al^{3+} = 0.675 Å) [24].

Table 1. Structural parameters of the freshly synthesized materials. Elemental composition and textural properties for the calcined materials. The numbers in brackets are nominal values.

Catalyst	Structural parameters of the freshly synthesized materials		Elemental composition of the calcined materials			Low temperature nitrogen sorption of the calcined materials		
	c [A][a]	a [A][b]	Ni [wt.%]	Y [wt.%]	M^{2+}/M^{3+}[−]	S_{BET}[m^2/g][c]	V_p[cm^3/g][d]	d_p[nm][e]
Ni-DLH	23.45	3.06	20	–	3.6 (3.0)	120	0.5	19
NiY3-DLH	23.54	3.06	17	2.8 (3.0)	3.8 (3.0)	142	0.5	13
NiY4-DLH	23.51	3.06	16	3.4 (4.0)	3.7 (3.0)	153	0.7	18
NiY8-DLH	24.02	3.08	13	5.6 (8.0)	3.8 (3.0)	81	0.2	11

a Calculated from (110) spacing $a = 2d_{(110)}$, as described by Cavani et al. [19].

b Calculated from XRD patterns of the fresh catalysts, from the position of the three first reflections $c = d_{(003)} + 2d_{(006)} + 3d_{(009)}$, as described by Cavani et al. [19].

c Specific surface areas calculated from the BET equation.

d Mesopore volumes derived from the BJH desorption calculation method.

e Pore size distribution obtained from the BJH desorption calculation method.

Fig. 2 presents XRD patterns of the calcined materials, showing reflections of Ni-Mg-Al periclase-mixed oxides (ICDD 00-045-0946) (2θ ca. 36.7°, 43° and 62.5°), which are characteristic for double-layered hydroxides after calcination [26,29]. For the NiY3-DLH catalyst calcination at 550 °C resulted in the stabilization of the $Mg_6Al_2(OH)_{16}CO_3 \cdot 4H_2O$ phase (ICDD 00-014-0191), as evidenced by reflections at 2θ of ca. 11°, 22° and 35°, corresponding to crystal planes of (0 0 3), (0 0 6), (0 0 9), respectively [15,18,24]. None such effect was observed for NiY4-DLH and NiY8-DLH catalysts. For the latter, the separate yttrium phase was registered as Y_2O_3 (ICDD 01-074-1828) (2θ ca. 29.3°, 33.9°, 39.0°, 48.8°, 57.9°).

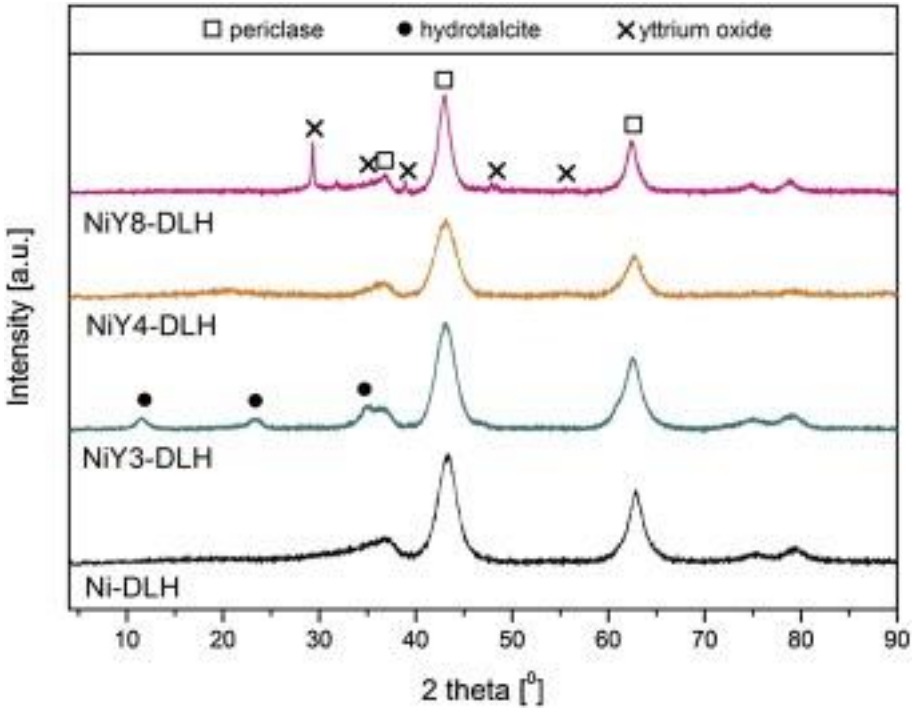

Fig. 2. XRD patterns of the calcined catalysts Ni-DLH, NiY3-DLH, NiY4-DLH, and NiY8-DLH.

Elemental analysis is listed in Table 1. The unmodified catalyst contained 20 wt.% of Ni, while the nickel content was decreasing with the increasing loading of yttrium for NiY-DLHs samples. Similar observation was registered by Wang et al. [30]. The lower nickel content for Y-modified samples may arise from possible substitution of Ni^{2+} by Y^{3+}, as suggested by Li et al. [31] for Y_2O_3-Ni/SBA-15 catalysts. In the latter case, the ion exchange can promote the generation of oxygen vacancies, positively affecting catalytic stability due to elimination of carbon deposit. The detected contents of yttrium for NiY3-DLH and NiY4-DLH were close to the nominal values, i.e., 2.8 and 3.4 wt.%. An exception was observed for NiY8-DLH catalyst, revealing 5.6 wt.% which is much lower than assumed 8 wt.%. The calculated ratios of M^{2+}/M^{3+}, i.e., (Ni + Mg)/(Al + Y), were relatively close to the values which were assumed during the synthesis step for all the samples.

All the Ni and Y-modified samples are mesoporous materials with S_{BET}(maintained after calcination) between 81 and 153 m^2/g (Table 1). The modification with 3 and 4 wt.% of yttrium led to increase of specific surface area as compared to unmodified catalyst. Similar effect was observed in our previous study for 0.6 and 1.5 wt.% for which 162 and 192 m^2/g was registered, respectively [16]. For NiY8-DLH catalyst, however, a significant decrease was observed for S_{BET}, V_p, and d_p. This loss may be explained by deposition of Y_2O_3on the outer surface, as

confirmed by XRD. The mesopores volume was 0.5 cm^3/g for unmodified and NiY3-DLH catalysts, while introduction of 4 wt.% led to the slight increase of this parameter, i.e. 0.7 cm^3/g. Modification with 4 wt.% of yttrium also resulted in an increased pore diameter as compared to NiY3-DLH. The lower textural parameters observed for NiY3-DLH sample, in comparison to NiY4-DLH, may lay in the existence of rest hydrotalcite phase in the former, which did not turn to nano-oxides during calcination.

3.2. Reducibility, basicity, Ni dispersion and crystallite size

TPR-H_2 profiles of studied Y-modified catalysts are presented in Fig. 3. The profile for Ni-DLH shows two wide peaks with maxima at 386 and 829 °C, respectively, which may be attributed to NiO weakly-bonded to the mixed oxides structure and NiO interacting strongly with the mixed oxide support, respectively [15,16,32]. The former almost disappeared with the assumed Y loadings of 3.0 and 4.0 wt.%, as compared to unmodified catalyst. Similarly, as for Ni-DLH, the Y3 and Y4 catalysts revealed presence of broad TPR peak at 823 and 856 °C, respectively. A distinctive reducibility behavior was observed for NiY8-DLH. For this catalyst, a significant contribution of bulk NiO species was registered with two intensive peaks at 460 and 494 °C [33]. Moreover, a shoulder at 605 °C was also observed, which may be linked with the reduction of nickel species of medium-strength. A broad peak at ca. 744 °C was also recorded, arising from NiO species strongly interacting with the mixed oxide support. In all studied materials, nickel oxides cannot be completely reduced to Ni° as high temperature peaks did not end in a flat line. According to Hu et al. [34] it is almost impossible to reduce the Ni–O–Mg species, which obviously were present in our materials due to recorded periclase structure of Mg(Ni,Al)O nano-mixed oxides. Sun et al. [35] reported that addition of yttrium (5, 8 and 10 wt.%) to Ni/γ-Al_2O_3 led to widening of TPR peaks and their shift to the lower temperatures. The authors claimed that yttrium modification not only increased the reducibility of the Ni-alumina catalysts, but also hindered formation of $NiAl_2O_4$ spinel. This phase was not observed in our conditions. Furthermore, yttrium oxide cannot be reduced in our TPR-H_2 conditions [36], however, possible NiO-Y_2O_3 interactions could have contributed to the observed changes. The latter are found in most of the oxides supported metal catalysts [30,37]. Clearly the total reduction area for NiY8-DLH sample is the highest among the studied catalysts. This may be attributed to the enhanced number of NiO formed upon modification with yttrium. Thus, oxygen vacancies, arising from Y_2O_3, may contribute to this effect.

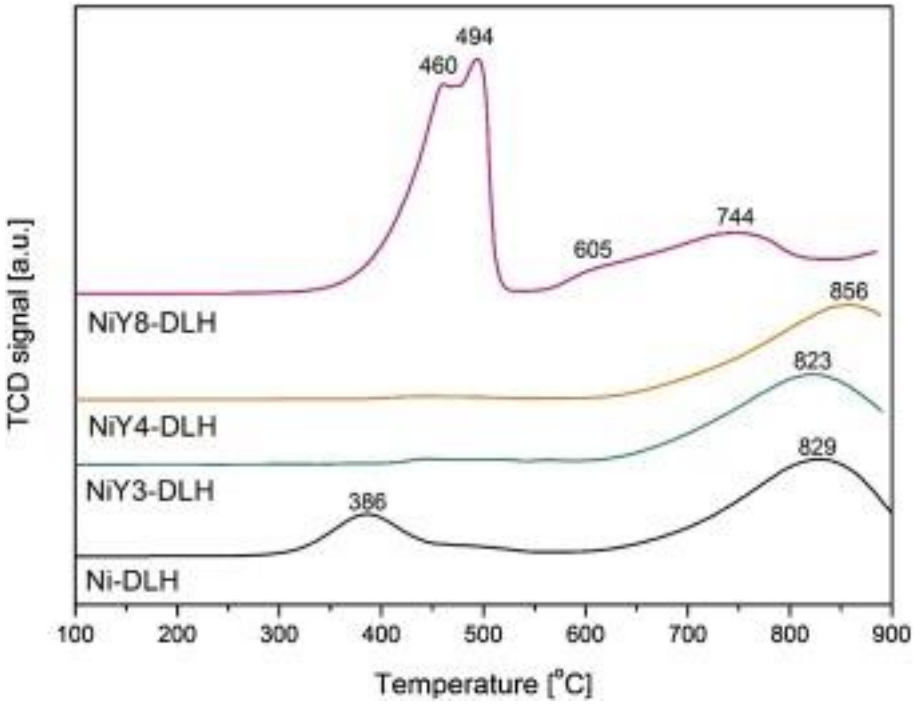

Fig. 3. Temperature-programmed reduction in H_2 (TPR-H_2) profiles of the calcined catalysts.

Fig. 4 shows XRD diffractograms of the reduced catalysts, in which characteristic metallic nickel phase (ICDD 01-087-0712) is evidenced by the presence of reflections at 2θ ca. 44.5°, 53°, 76.5°, corresponding to crystal planes of (1 1 1), (2 0 0), (2 2 0). Also, a periclase-mixed oxides phase (2θ ca. 36.7°, 43°, 62.5°) is observed [13,38]. Table 2 presents the calculated values of Ni° crystallites, calculated from the 2θ diffraction peak at ca. 53° (corresponding to (2 0 0) crystal plane of Ni°) using the Scherrer equation. It may be seen that the 3 wt.% of yttrium addition did not influence the size of Ni° crystallites, as 8 nm was calculated for both Ni-DLH and NiY3-DLH. Only a slightly smaller value was registered for the NiY4-DLH sample (6 nm). The promotion with assumed 8 wt.% of yttrium led to particles of Ni being twice larger than those of the Ni-DLH and NiY3-DLH catalysts (15 nm vs. 8 nm).

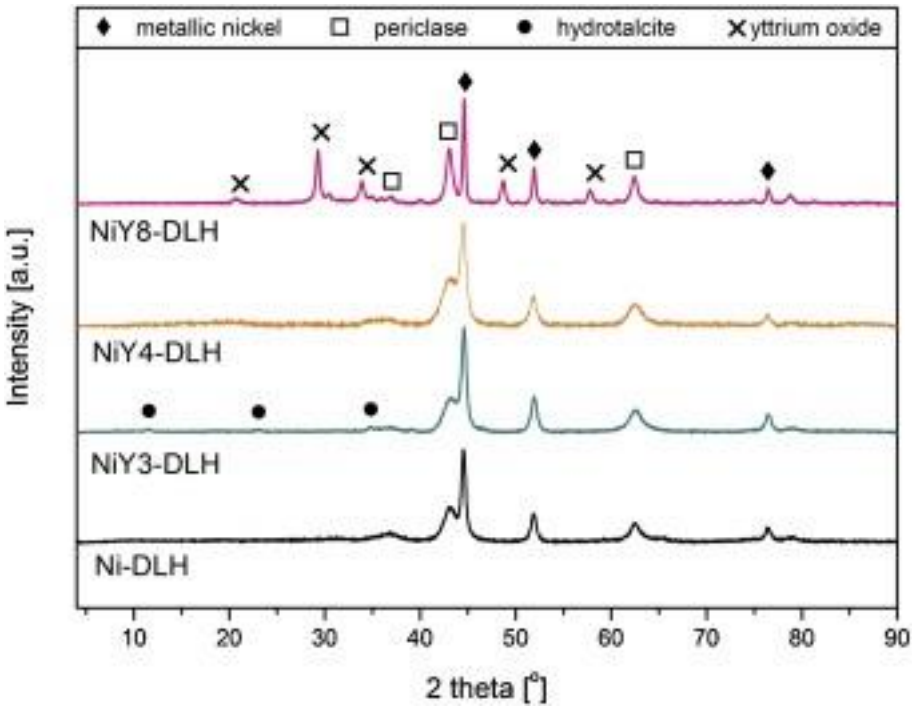

Fig. 4. XRD patterns of the reduced catalysts Ni-DLH, NiY3-DLH, NiY4-DLH, and NiY8-DLH.

Table 2. The number of basic sites and their percentage distribution derived from TPD-CO_2.

Catalyst	XRD	TPD-CO_2						
	Ni° crystallite size [nm]	Number of basic sites [μmol/g]				Percentage distribution [%]		
	$d_{Ni°}$ [a]	I: Weak	II: Medium	III: Strong	Total basicity	I: Weak	II: Medium	III: Strong
Ni-DLH	8	16	44	46	107	15	41	43
NiY3-DLH	8	–	106	66	173	–	62	38
NiY4-DLH	6	41	92	91	224	18	41	41
NiY8-DLH	15	59	127	78	265	22	48	30

[a] Based on the Scherrer equation, from the width at half-maximum of the XRD reflections at 2θ ca. 53°.

Basicity of the reduced catalysts was studied by TPD-CO_2. Since carbon dioxide has mild acidity, basic supports are advantageous for CO_2 to adsorb on the surface [39]. The obtained profiles are shown in Fig. 5. Three types of basic sites can be distinguished considering the

temperature zone where CO_2desorption takes place. The lowest temperature region describes the weak basic sites (I) arising from Brønsted hydroxyl groups. At the moderate temperatures, the sites with medium-strength (II) can be recognized which are known as Lewis acid-base sites. The CO_2 desorbs from strong basic sites (III) at the highest temperature, and they are associated with Lewis basic sites with oxygen anions [[15], [16], [17], [18]].

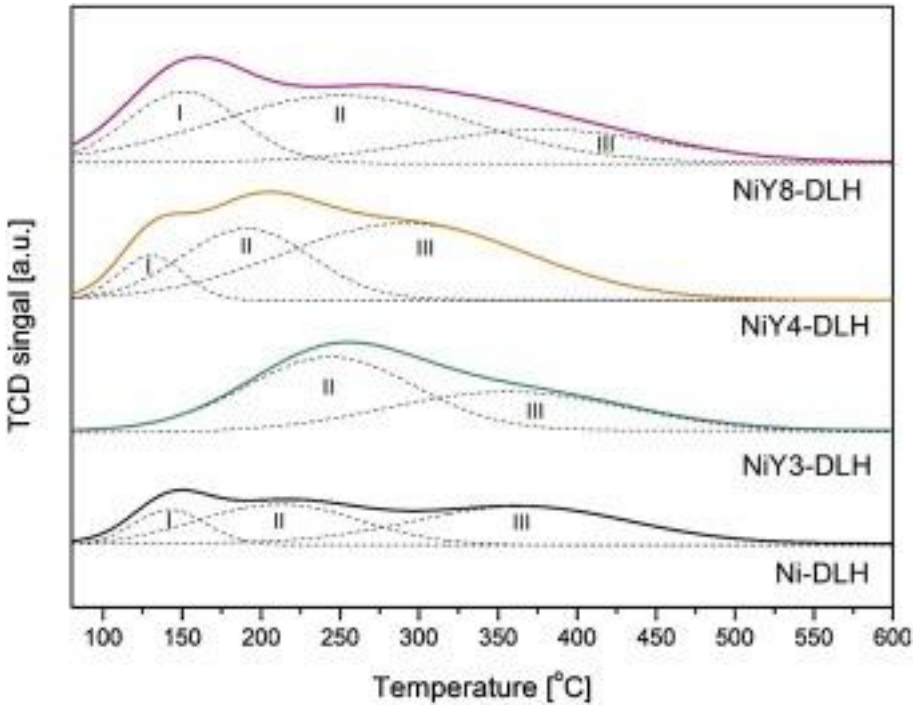

Fig. 5. Temperature-programmed desorption of CO_2 (TPD-CO_2) profiles for the reduced materials.

The total basicity gradually increased with the increasing content of yttrium, showing the highest value of 265 μmol/g for NiY8-DLH. The leftward shift of weak basic sites was observed for NiY4-DLH and NiY8-DLH catalysts leading to formation of new sites which amount was increasing with Y content (Table 2). The NiY3-DLH catalyst revealed different basicity distribution among others. A shift to stronger basic sites was recorded, significantly increasing a number of medium ones, and leading to an absence of weak sites. This may be linked to the presence of rest hydrotalcite phase in the calcined and reduced NiY3-DLH. For NiY4-DLH, only a slight decrease of medium basic sites was observed as compared to NiY3-DLH. On the other hand, for the sample with assumed 8 wt.% of yttrium a significant increase of number of sites with medium-strength was recorded in comparison to Y4 material. This can be attributed to the existence of a separate Y_2O_3 phase on the calcined and reduced NiY8-DLH, offering new medium-strength basic sites. In our former studies, we recorded a shift towards

lower CO_2 desorption temperatures with increasing yttrium content [15,16]. This shift is also present in TPD-CO_2 profiles of NiY4-DLH catalyst. Comparing all series of Y-containing mixed-oxides, a distinctive behavior may be observed for NiY3-DLH and NiY8-DLH samples, as these catalysts revealed different structural properties as mentioned above.

The addition of Y modified also distribution of basic sites as shown in Table 2. The highest percentage of medium basic sites, calculated for the studied catalysts, was obtained for NiY3-DLH material at the expense of the weak sites. Moreover, NiY8-DLH revealed 48 % of medium-strength basicity, whereas Ni-DLH and NiY4-DLH samples showed the same value of 41 %. The contribution of medium basic sites is considered to be of advantage for dry reforming for methane reaction rather than the strong sites. A proper basicity hinders carbon formation and/or contributes to oxidation of formed coke [39]. In contrast, too strong CO_2 adsorption, which results in carbon formation, originates from the presence of the strongest basic sites.

3.3. Catalytic performance in DRM

Fig. 6A–C show the dry reforming of methane over studied catalysts, assuming isothermal steady-state conditions at 700 °C. The catalytic activity presents the following sequence: NiY8-DLH < Ni-DLH < NiY3-DLH ~ NiY4-DLH. The average conversion values for Y-promoted catalysts are listed in Table 3. All studied materials revealed relatively stable conversion values for 5 h, with the CO_2conversions higher than for CH_4. This arises from side reactions occurrence, such as reverse water gas shift (RWGS), which allows to convert more carbon dioxide, and consequently produce excess of CO. This is in line with low H_2/CO ratios lower than unity recorded for all catalysts, expect for NiY4-DLH for which average molar ratio of H_2/CO was 1.0. The trends discussed above are in good agreement with those reported in literature for other Y-promoted DRM catalysts [[15], [16], [17], [18]]. Additionally, other side reactions such as gasification of carbon deposits and the Boudouard reaction could have also taken place [13,40]. Moreover, in the study of Ojeda-Niño et al. [41] a series of Ni-Mg-Al hydrotalcites were synthesized by the microwave-assisted self-combustion method and promoted by different concentrations of praseodymium, i.e., 1.2 wt.%, 5.9 wt.% and 11.4 wt.%. In the first 5 h of DRM test, the activity was presenting the following sequence at 600 °C: OM2 (5.9 %) < OM0 (no Pr) < OM1 (1.9 %) ~ OM3 (11.4 %). The OM2 catalyst with the lowest CH_4 and CO_2conversions values revealed the lowest formation of carbon deposits. The

observation reported by the authors may be in line with our results, considering that elemental analysis showed 5.6 wt.% of yttrium in NiY8-DLH sample.

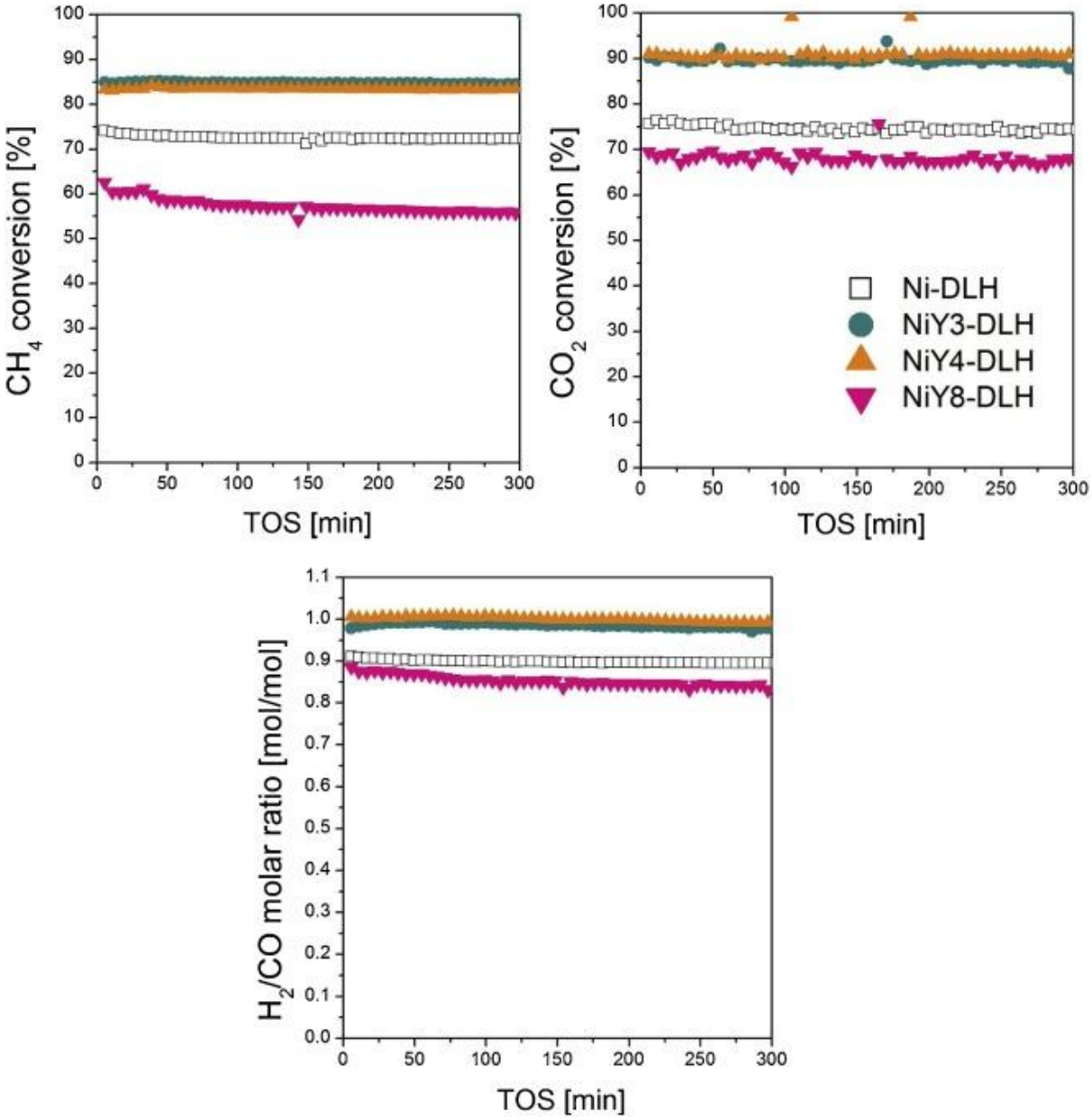

Fig. 6. Catalytic activity of NiY-DLH catalysts (with assumed 3.0, 4.0 and 8.0 wt.% of yttrium) in the isothermal experiments: CH_4 conversion, CO_2 conversion, and H_2/CO molar ratio versus TOS (time on stream) in DRM process ($CH_4/CO_2/Ar = 1/1/8$, 700 °C, GHSV = 20,000 h^{-1}).

Table 3. Comparison between literature results obtained for dry reforming of methane (gas mixture of $CH_4/CO_2/Ar = 1/1/8$, GHSV = 20,000 h^{-1}, total flow rate = 100 ml/min).

Studied catalyst	Average values obtained at 700 °C			References
	CH_4 conversion [%]	**CO_2 conversion [%]**	**H_2/CO molar ratio [−]**	
Ni-Mn/Ce50-Zr50	62.3	65.8	0.87	[43]
Ni-Mo/Al_2O_3	50.0	60.6	0.74	[44]
Ni–10Mg/Fe-clay	50	60	0.75	[45]
15 %Ni/Ce-Zr-Y	87	86	1.02	[46]
HTNi/ZrY0.4	82	79	0.85	[17]
HT Ce/Y0.4	82	83	0.95	[18]
NiY3-DLH	85	90	0.99	This study
NiY4-DLH	84	90	1.0	This study
NiY8-DLH	58	68	0.87	This study

After yttrium modification, as studied in this paper, the specific surface areas increased. A certain correlation may be observed, as catalytic activities of the studied materials were directly related to their surface areas, i.e., higher S_{BET} led to higher catalytic activity in dry reforming of methane. However, the DRM reaction does not always depend on this parameter, and generally, it is not crucial in terms of catalytic behavior. One example may be the work of Barroso-Quiroga et al. [42] who studied Ni/α–Al_2O_3 (3.3 m^2/g) and Ni/γ–Al_2O_3 (150 m^2/g) performing with similar catalytic activity, i.e., 34.7 % and 36.6 % of maximum CO_2 conversion at 550 °C, respectively. The dominant factors for the enhanced activity in DRM are Ni° crystallite size, basicity and reducibility. According to the DRM mechanism, these three factors greatly influence the conversion of $CH_4$and CO_2 into H_2 and CO. In current study, the XRD showed the lowest Ni° crystallite size for NiY4-DLH catalyst, which in DRM test revealed the highest CO_2 and CH_4 conversions. The results of TPD-CO_2 revealed that the highest share of medium basic sites was found in NiY3-DLH. This could also have contributed to the high catalytic activity for this catalyst. From the TPR-H_2, the increased number of reducible NiO species was registered for NiY8-DLH in comparison to the other studied catalysts. This implies that possibly more lattice oxygen ions are supplied to the DRM reaction over the NiY8-DLH catalyst. Simply, more oxygen vacancies could be formed on the surface which subsequently

contributed to the hindering of carbon formation [30]. The resistance to carbon formation will be supported in the section dedicated to characterization of the spent catalysts.

The catalytic results of the studied catalysts were compared to those reported in other literature studies. The average values of CH_4 and CO_2 conversions, as well as, H_2/CO molar ratio are presented in Table 3. The reaction conditions are the same in all the provided examples of the studies, which makes a direct comparison possible. For Ni–Mn/Ce50-Zr50, the conversions of CH_4, CO_2, and the ratio of H_2/CO were 62.3 %, 65.8 %, and 0.87, respectively. Lower values were recorded for both nickel and molybdenum modified alumina and Ni–10Mg/Fe-clay, giving ca. 50 %, 60 % and 0.74 of CH_4 and CO_2 conversions, and H_2/CO molar ratios, respectively.

The presence of yttrium positively influenced the catalytic behavior showing more than 80 % of CO_2 conversion, and from 79 to 90 % of CH_4 conversion. The catalytic results were slightly lower for NiY8-DLH sample, reaching the values similar to those recorded for Ni–Mn/Ce50-Zr50 and Ni-Mo/Al_2O_3 catalysts.

3.4. Characterization of the spent catalysts

XRD diffractograms were recorded for the spent catalysts in order to examine the Ni° crystallite size, the possible changes in the support after the catalytic process, and the carbon formation. The results are presented in Fig. 7, where reflections typical for metallic nickel phase (ICDD 01-087-0712) and periclase-like mixed oxides phase can be found (ICDD 00-045-0946) [13,38], similarly as for the reduced catalysts (cp. Fig. 4). Crystallite size of Ni° did not change significantly after the tests, as for all catalysts the values are close to those recorded for the reduced (cp. Table 2). This suggests the lack of sintering of the nickel particles upon high temperature applied during DRM. Additionally, the reflections of graphite carbon (ICDD 01-075-2078) at $2\theta = 26.6°$ were registered for all catalysts, except for NiY8-DLH. Thus, the latter seems to be the most stable material due to enhanced resistance to the coke formation. For the Ni-DLH catalyst reflections of $Mg_6Al_2(OH)_{16}CO_3 \cdot 4H_2O$ (ICDD 00-014-0191) were also registered at $2\theta = 11.5$ and 22.9°. This phase is typical for DLHs after synthesis and before calcination at around 500 °C [47]. The presence of hydrotalcite phase was reported before for Ni-based DLHs after DRM tests, and indicates a partial regeneration of the support in the presence of water. This property, so-called memory effect of DLHs, facilitates reconstruction of mixed oxides to the original DLHs phase or meixnerite [48,49]. The reflections of

$Mg_6Al_2(OH)_{16}CO_3 \cdot 4H_2O$ were not observed in the spent NiY3-DLH, in contrast to both the calcined (cp. Fig. 2) and the reduced catalysts (cp. Fig. 4). A possible explanation could be that the catalyst was fully transformed into the periclase phase during dry reforming of methane experiment, and the occurrence of side reactions did not lead to the partial regeneration of hydroxides.

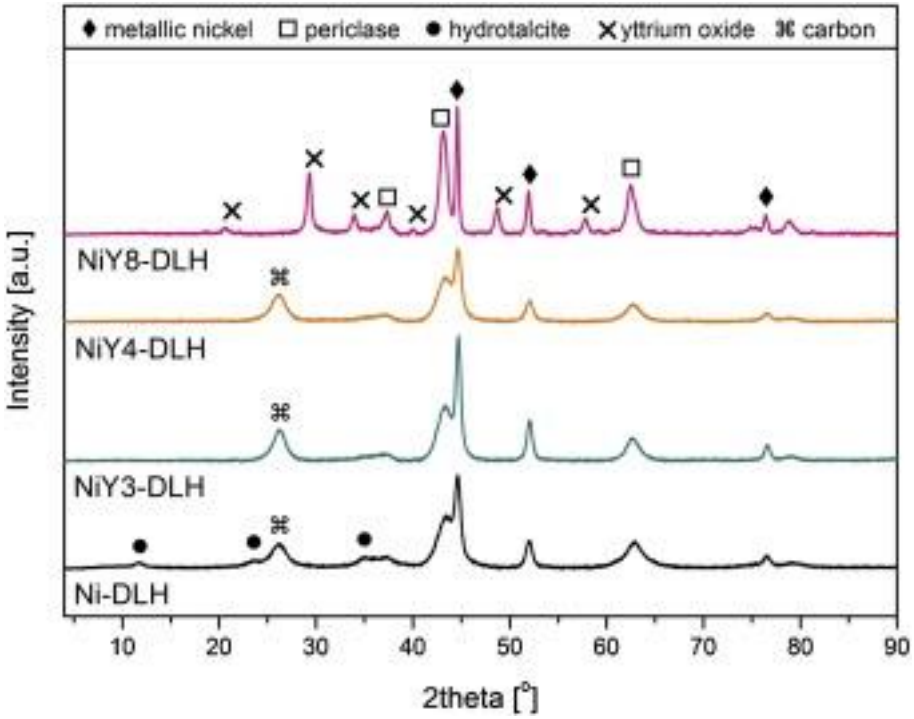

Fig. 7. XRD patterns of the catalysts after dry reforming of methane experiments ($CH_4/CO_2/Ar = 1/1/8$, 700 °C for 5 h).

In order to examine the properties of carbonaceous species on the spent catalysts Raman spectroscopy was used. For Ni and the Y-promoted DLHs, four bands were registered: D band, G band, D' band and G' band (Fig. 8). The D and D′ bands arise from a disorder in graphite structure and they were ascribed to the non-zone centered phonons associated to the disorder-induced vibration of C-C bond. The G and G′ bands refer to the stretching vibrations in the aromatic layers of graphite and they are only present in perfect crystalline graphite [50]. Table 4 shows the calculated ratios of the intensity of D and D' bands to the intensity of G and G' bands, I_D/I_G, which describe the graphitization degree of carbon and the disorder in its structure. The relative intensity of the D and G bands (I_D/I_G) gives valuable information about the crystallinity degree of the carbon formed during the DRM. The lower I_D/I_G ratio refers to a high crystallinity and high graphitization degree due to the higher contribution of the graphitized carbon fractions formed [51,52]. The Y-modified materials showed decreasing I_D/I_G ratios with

1.83 for Ni-DLH versus 0.84 and 1.06 for NiY3-DLH and NiY4-DLH, respectively (Table 4). Therefore, it can be concluded that different carbon structures were formed on the studied catalysts, and the carbon deposited on Y promoted materials (with assumed 3.0 and 4.0 wt.%) is more graphitic as compared to unmodified sample. The graphitic-type of carbon is mainly responsible for deactivation, and acts like a shell covering the Ni particle layer by layer [40,53]. This later result shows that promotion with 3 and 4 wt.% of yttrium influenced the DRM mechanism in favoring side reactions, such as for example direct methane decomposition or Boudouard reaction. For NiY8-DLH, however, no peaks in Raman spectrum were registered. This latter result again confirms superior coke resistance when yttrium loading was assumed as 8 wt.%.

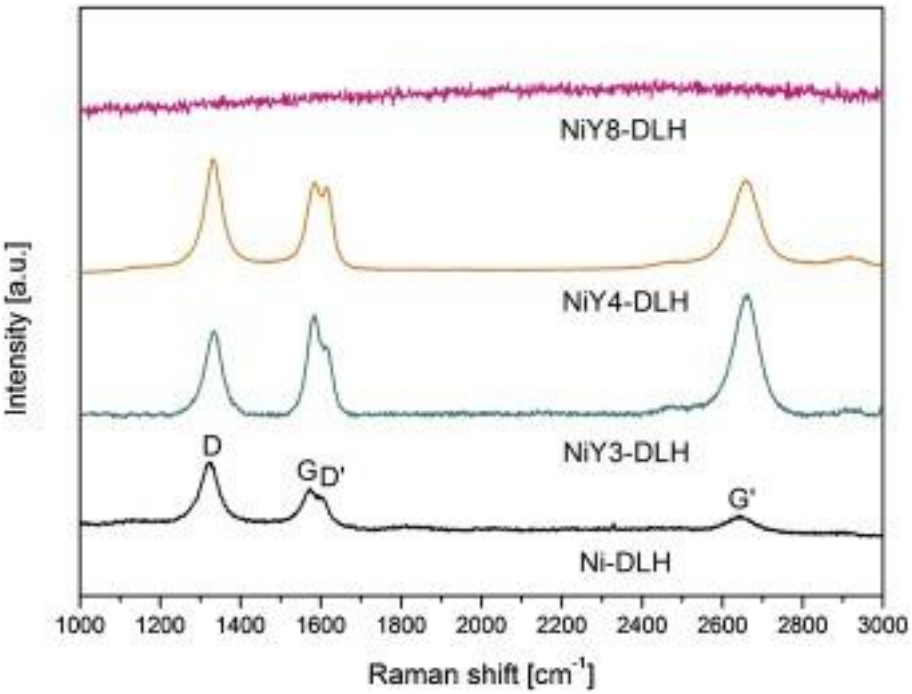

Fig. 8. Raman spectra of the spent catalysts ($CH_4/CO_2/Ar = 1/1/8$, 700 °C for 5 h). The I_D/I_G ratio describes the degree of crystallinity of the formed carbon.

Table 4. Properties of the spent catalysts: Ni^0 crystallite size, I_D/I_G intensity ratio obtained from Raman spectrum, and the mass loss registered in thermogravimetric analysis. The parenthesis "{}" includes the data recorded for reduced samples, taken from Table 2.

Catalyst	**XRD**	**Raman**	**TGA**
	Ni^0 crystallite size [nm][a]	**I_D/I_G [−]**	**Total mass loss [%]**
Ni-DLH	7 {8}	1.83	26.1
NiY3-DLH	8 {8}	0.84	35.1
NiY4-DLH	5 {6}	1.06	39.9
NiY8-DLH	14 {15}	no bands	23.0

[a] Based on the Scherrer equation, calculated from the half-width of the XRD reflections at 2θ ca. 53°.

TGA curves are presented in Fig. 9, where 26.1, 35.1, 39.9 and 23.0 % total weight losses were recorded for Ni-DLH, NiY3-DLH, NiY4-DLH and NiY8-DLH, respectively. The samples were decomposed while increasing temperature, and their weight loss is mainly attributed to removal of water, residues, desorption of CO_2, and/or oxidation of carbonaceous species [13,54]. The latter are found in Ni-DLH, NiY3-DLH and NiY4-DLH spent catalysts, and three regions of carbon removal may be distinguished basing on the oxidation temperature: (i) amorphous carbon ($T < 300$ °C), (ii) filamentous carbon (400–700 °C), and (iii) graphite (>800 °C) [[54], [55], [56]]. According to Zhang et al. [57] amorphous carbon can participate in the formation of synthesis gas via gasification with CO_2or H_2O, while graphite leads to catalysts deactivation. Additionally, a slight increase of the mass may be observed at 300 °C for the unpromoted catalyst, arising from re-oxidation of Ni° [58]. In case of carbon-free NiY8-DLH, the weight decrease could have arisen from some part of carbon which amount and character was different in comparison to the deposit observed for other catalysts. The lowest mass loss was registered for spent NiY8-DLH, as showed in Table 4.

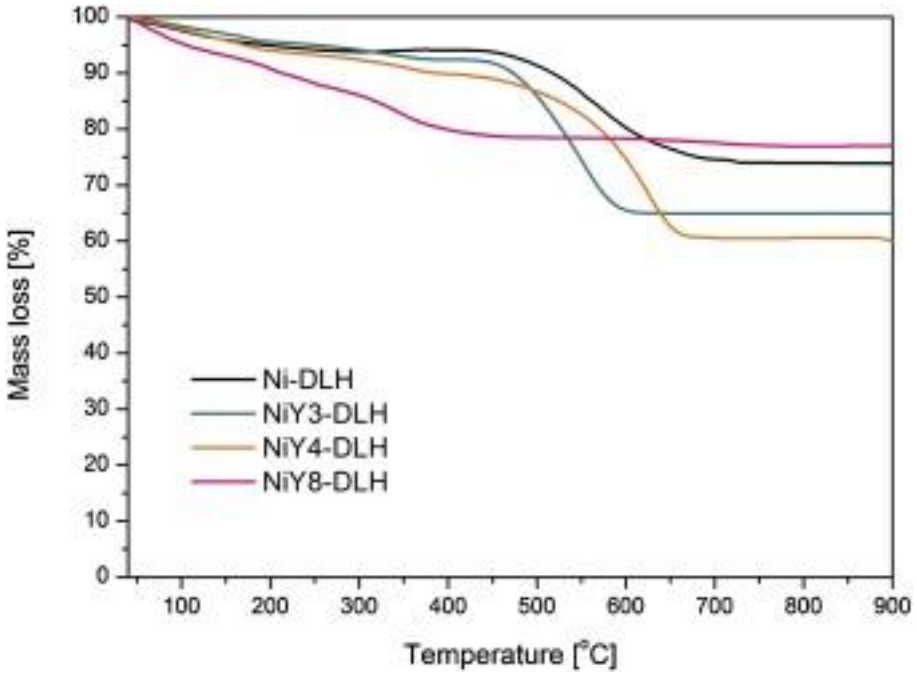

Fig. 9. TGA over the spent catalyst (CH_4/CO_2/Ar = 1/1/8, 700 °C for 5 h).

High-resolution electron microscopy was carried out to study the distribution of the Ni particle size, presence of carbonaceous species, and existence of yttrium compounds. Fig. 10 shows the HRTEM images of the used catalysts Ni-DLH and NiY8-DLH. The red circled spots represent particles of metallic Ni. It may be clearly seen that their size for Ni-DLH is much lower as compared to the ones for NiY8-DLH (average value for the former: 14 nm, and the latter: 59 nm). Furthermore, the blue circled spot, indicated in micrographs of Ni-DLH sample, presents laminar structure of hydroxides. This is in line with XRD results (cp. Fig. 7), where reflections of $Mg_6Al_2(OH)_{16}CO_3{\cdot}4H_2O$ were registered. EDS was also performed for NiY8-DLH catalyst in order to identify the nature of particles. The obtained EDS spectra confirmed the presence of nickel particle in the direct vicinity to yttrium particle. This shows that the two elements do not form a compound, nor a spinel, which is in line with XRD results. One of the micrographs confirms presence of a Y_2O_3 particle with an interarticular distance d_{hkl} of 2.67 Å corresponding to a (4 0 0) plane. This is again in good agreement with recorded X-ray diffractograms for calcined and reduced materials.

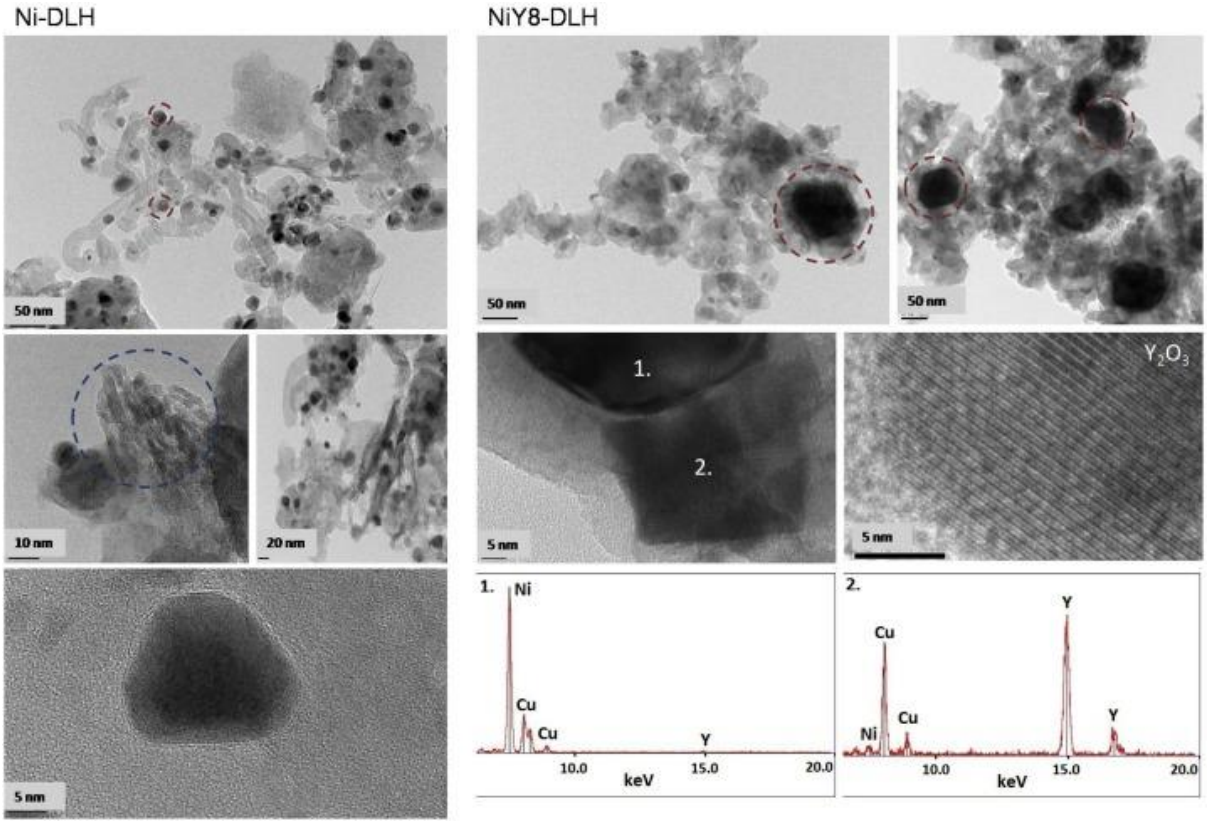

Fig. 10. HRTEM micrographs of spent Ni-DLH and NiY8-DLH catalysts.

Fig. 11A, B present EDS elemental mapping performed for NiY8-DLH catalyst after dry reforming of methane test. The images confirm the presence of constructive elements of material (Mg, Ni, O, Y, Al). It can be observed that the catalyst is of non-uniform morphology and includes large Ni particles, as well as, well-distributed nanoparticles. Those former seem to be inactive in our catalytic reaction, as it is well known that a large size of metallic nickel facilities a high selectivity towards carbon formation. In turn, the observed Ni nanoparticles could extensively participate in the DRM catalytic test, being non-selective towards coke formation. The yttrium element was found to be homogeneously dispersed over the support, which could also positively influence the carbon removal, considering yttrium oxide as a source of oxygen vacancies.

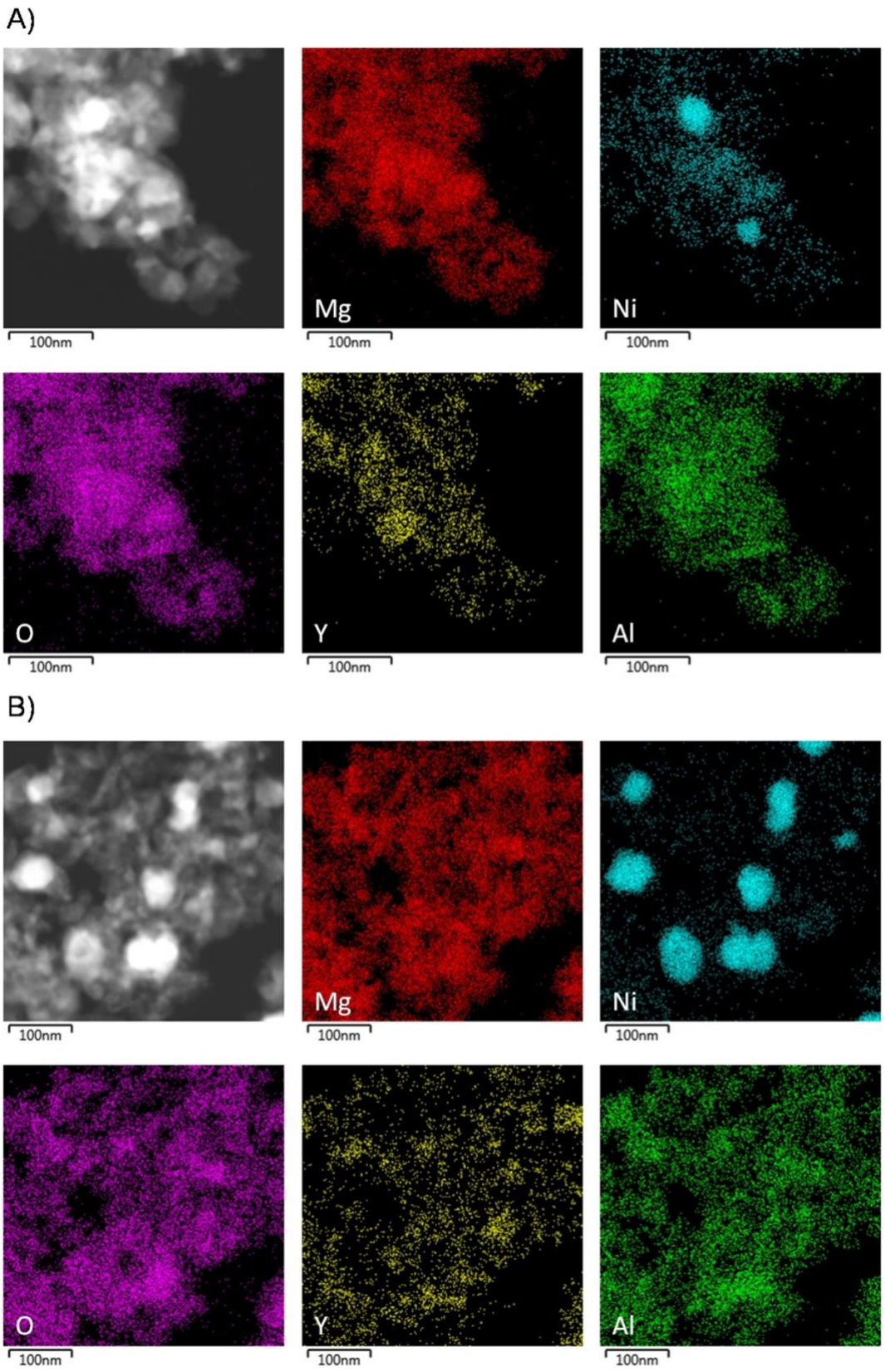

Fig. 11. EDS elemental mapping images of NiY8-DLH recorded at two different spots of the specimen (A, B).

4. Conclusions

In this study, Ni-containing Mg/Al double-layered hydroxides (DLHs) synthesized by co-precipitation method were promoted with Y assuming 3.0, 4.0, or 8.0 wt.%, and compared to a non-promoted catalyst. The nanostructured catalysts were composed of a homogeneous solid periclase structure of Mg(Ni, Al)O nano-mixed oxides, while modification with assumed 8 wt.% of yttrium led to presence of Y_2O_3 separate phase, well-dispersed on the surface. Ni-DLH and NiYx-DLH (x = 3, 4, 8) catalysts were tested in dry reforming of methane (DRM) in the isothermal tests at 700 °C for 5 h. All the catalysts were active in the DRM, without a direct correlation to the Y content in conversion. The highest catalytic activity was found on NiY4-DLH catalyst, which can be directly linked with the lowest Ni° crystallite size observed by XRD. NiY3-DLH catalyst showed equally good results in DRM, and its performance may be connected with the highest amount of medium basic sites. Both catalysts, however, suffered from deactivation due to the carbon formation. It was found that an assumed amount of Y of 8 wt.% improves the catalytic stability as carbon formation was hardly revealed by XRD, HRTEM and Raman techniques. The yttrium loading of 8 wt.% facilitated the reduction of Ni species and increase of total basicity. The Ni crystallinity, however, increased as compared to other tested catalysts, leading to formation of big Ni particles probably inactive in dry reforming of methane and accompanying reactions. Second population of Ni particles was discovered by EDS elemental analysis, which proved well-distribution of nickel accessible to gaseous reactants. The carbon-free performance could be attributed to oxygen vacancies originating from well distributed Y_2O_3, allowing more efficient gasification of carbon deposits.

Acknowledgments

The French Embassy in Poland and InnoEnergy PhD School are gratefully acknowledged for the financial support of K. Świrk during her co-tutelle doctoral studies at Sorbonne Université. K. Świrk would also like to express her gratitude to the KinCat Catalysis Group at NTNU for the possibility to conduct this research during her Erasmus + traineeship. The authors would like to acknowledge Patricia Beaunier (Sorbonne Université) for HRTEM expertise and EDS

elemental mapping. M. Motak would like to acknowledge the support of AGH grant 16.16.210.476.

References

[1] J. Gao, Z. Hou, H. Lou, X. Zheng, Dry (CO_2) Reforming, First Edit, Elsevier, 2011. doi:10.1016/B978-0-444-53563-4.10007-0.

[2] J. Yang, W. Ma, D. Chen, A. Holmen, B.H. Davis, Fischer-Tropsch synthesis: A review of the effect of CO conversion on methane selectivity, Appl. Catal. A Gen. 470 (2014) 250–260. doi:10.1016/j.apcata.2013.10.061.

[3] Z. Zhang, X.E. Verykios, A stable and active nickel-based catalyst for carbon dioxide reforming of methane to synthesis gas, J. Chem. Soc. Chem. Commun. (1995) 71–72. doi:10.1039/C39950000071.

[4] A. Goeppert, M. Czaun, J.P. Jones, G.K. Surya Prakash, G.A. Olah, Recycling of carbon dioxide to methanol and derived products-closing the loop, Chem. Soc. Rev. 43 (2014) 7995–8048. doi:10.1039/c4cs00122b.

[5] K. Świrk, M.E. Galvez, A. Izquierdo, M. Motak, P. Da Costa, T. Grzybek, Thermodynamic equilibrium analysis of methane reforming as a prospective process for synthesis gas production, in: Contemp. Probl. Power Eng. Environ. Prot., 2016: pp. 169–177.

[6] EUROPEAN COMMISSION, Critical raw materials, 2014 (2016). https://ec.europa.eu/growth/sectors/raw-materials/specific-interest/critical_en.

[7] L. Zhang, X. Wang, C. Chen, X. Zou, X. Shang, W. Ding, X. Lu, Investigation of mesoporous $NiAl_2O_4/MO_x$ (M = La, Ce, Ca, Mg)–γ-Al_2O_3 nanocomposites for dry reforming of methane, RSC Adv. 7 (2017) 33143–33154. doi:10.1039/C7RA04497F.

[8] F. Pompeo, N.N. Nichio, M.G. González, M. Montes, Characterization of Ni/SiO_2 and $Ni/Li-SiO_2$ catalysts for methane dry reforming, Catal. Today. 107–108 (2005) 856–862. doi:10.1016/j.cattod.2005.07.024.

[9] A.S. Al-Fatesh, A.A. Ibrahim, J.K. Abu-Dahrieh, A.S. Al-Awadi, A.M. El-Toni, A.H. Fakeeha, A.E. Abasaeed, Gallium-promoted Ni catalyst supported on MCM-41 for dry reforming of methane, Catalysts. 8 (2018) 1–14. doi:10.3390/catal8060229.

[10] X. Huang, G. Xue, C. Wang, N. Zhao, N. Sun, W. Wei, Y. Sun, Highly stable mesoporous $NiO–Y_2O_3–Al_2O_3$ catalysts for CO_2 reforming of methane: effect of Ni embedding and Y_2O_3 promotion, Catal. Sci. Technol. 6 (2016) 449–459. doi:10.1039/C5CY01171J.

[11] B. Li, W. Su, X. Wang, X. Wang, Alumina supported Ni and Co catalysts modified by Y_2O_3 via different impregnation strategies: Comparative analysis on structural properties and catalytic performance in methane reforming with CO_2, Int. J. Hydrogen Energy. 41 (2016) 14732–14746. doi:10.1016/j.ijhydene.2016.06.219.

[12] B. Li, S. Zhang, Methane reforming with CO_2 using nickel catalysts supported on yttria-doped SBA-15 mesoporous

materials via sol-gel process, Int. J. Hydrogen Energy. 38 (2013) 14250–14260. doi:10.1016/j.ijhydene.2013.08.105.

[13] K. Świrk, M.E. Gálvez, M. Motak, T. Grzybek, M. Rønning, P. Da Costa, Syngas production from dry methane reforming over yttrium-promoted nickel-KIT-6 catalysts, Int. J. Hydrogen Energy. 44 (2019) 44. doi:10.1016/j.ijhydene.2018.02.164.

[14] Q. Wu, J. Chen, J. Zhang, Effect of yttrium and praseodymium on properties of $Ce_{0.75}Zr_{0.25}O_2$ solid solution for CH_4-CO_2 reforming, Fuel Process. Technol. 89 (2008) 993–999. doi:10.1016/j.fuproc.2008.03.006.

[15] K. Świrk, M. Motak, T. Grzybek, M. Rønning, P. Da Costa, Effect of low loading of yttrium on Ni-based layered double hydroxides in CO_2 reforming of CH4, React. Kinet. Mech. Catal. (2018). doi:10.1007/s11144-018-1515-9.

[16] K. Świrk, M.E. Gálvez, M. Motak, T. Grzybek, M. Rønning, P. Da Costa, Yttrium promoted Ni-based double-layered hydroxides for dry methane reforming, J. CO_2 Util. 27 (2018) 247–258. doi:10.1016/j.jcou.2018.08.004.

[17] K. Świrk, M.E. Gálvez, M. Motak, T. Grzybek, M. Rønning, P. Da Costa, Dry reforming of methane over Zr- and Y-modified Ni/Mg/Al double-layered hydroxides, Catal. Commun. 117 (2018) 26–32. doi:doi.org/10.1016/j.catcom.2018.08.024.

[18] K. Świrk, M. Rønning, M. Motak, P. Beaunier, P. Da Costa, T. Grzybek, Ce- and Y-modified double-layered hydroxides as catalysts for dry reforming of methane : On the effect of yttrium promotion, Catalysts. 9 (2019) 56–74. doi:10.3390/catal9010056.

[19] F. Cavani, F. Trifirò, A. Vaccari, Hydrotalcite-type anionic clays: Preparation, properties and applications., Catal. Today. 11 (1991) 173–301. doi:10.1016/0920-5861(91)80068-K.

[20] B. Wiyantoko, P. Kurniawati, T.E. Purbaningtias, I. Fatimah, Synthesis and characterization of hydrotalcite at different Mg/Al molar ratios, Procedia Chem. 17 (2015) 21–26. doi:10.1016/j.proche.2015.12.115.

[21] Y.F. Lung, Y.S. Sun, C.K. Lin, J.Y. Uan, H.H. Huang, Synthesis of Mg-Fe-Cl hydrotalcite-like nanoplatelets as an oral phosphate binder: Evaluations of phosphorus intercalation activity and cellular cytotoxicity, Sci. Rep. 6 (2016) 2–12. doi:10.1038/srep32458.

[22] P. Kuśtrowski, L. Chmielarz, E. Bożek, M. Sawalha, F. Roessner, Acidity and basicity of hydrotalcite derived mixed Mg-Al oxides studied by test reaction of MBOH conversion and temperature programmed desorption of NH_3 and CO_2, Mater. Res. Bull. 39 (2004) 263–281. doi:10.1016/j.materresbull.2003.09.032.

[23] J.T. Kloprogge, R.L. Frost, D. Chemistry, Thermogravimetric analysis-mass spectrometry (TGA-MS) of hydrotalcites containing CO_3^{2-}, NO^{3-}, Cl^-, SO_4^{2-} or ClO_4^-, in: A Clay Odyssey. Proc. 12th Int. Clay Conf. Bahai-Blanca, Argentina 2001, 2001. doi:10.1016/B978-044450945-1/50147-0.

[24] J.M. Fernández, C. Barriga, M.A. Ulibarri, F.M. Labajos, V. Rives, New hydrotalcite-like compounds containing yttrium, Chem. Mater. 9 (1997) 312–318. doi:10.1021/cm9603720.

[25] P. Gao, L. Zhong, L. Zhang, H. Wang, N. Zhao, W. Wei, Y. Sun, Yttrium oxide modified Cu/ZnO/Al_2O_3 catalysts via hydrotalcite-like precursors for CO_2 hydrogenation to methanol, Catal. Sci. Technol. 5 (2015) 4365–4377.

doi:10.1039/c5cy00372e.

[26] L. Chmielarz, P. Kuśtrowski, A. Rafalska-Łasocha, D. Majda, R. Dziembaj, Catalytic activity of Co-Mg-Al, Cu-Mg-Al and Cu-Co-Mg-Al mixed oxides derived from hydrotalcites in SCR of NO with ammonia, Appl. Catal. B Environ. 35 (2002) 195–210. doi:10.1016/S0926-3373(01)00254-5.

[27] O.D. Pavel, B. Cojocaru, E. Angelescu, V.I. Pârvulescu, The activity of yttrium-modified Mg,Al hydrotalcites in the epoxidation of styrene with hydrogen peroxide, Appl. Catal. A Gen. 403 (2011) 83–90. doi:10.1016/j.apcata.2011.06.017.

[28] J.M. García-García, M.E. Pérez-Bernal, R.J. Ruano-Casero, V. Rives, Chromium and yttrium-doped magnesium aluminum oxides prepared from layered double hydroxides, Solid State Sci. 9 (2007) 1115–1125. doi:10.1016/j.solidstatesciences.2007.07.029.

[29] C.E. Daza, S. Moreno, R. Molina, Co-precipitated Ni-Mg-Al catalysts containing Ce for CO_2 reforming of methane, Int. J. Hydrogen Energy. 36 (2011) 3886–3894. doi:10.1016/j.ijhydene.2010.12.082.

[30] Y. Wang, X. Hong, B. Li, W. Wang, D. Wang, Yttria promoted metallic nickel catalysts for the partial oxidation of methane to synthesis gas, J. Nat. Gas Chem. 17 (2008) 344–350. doi:10.1016/S1003-9953(09)60006-2.

[31] J.F. Li, C. Xia, C.T. Au, B.S. Liu, Y_2O_3-promoted NiO/SBA-15 catalysts highly active for CO_2/CH_4 reforming, Int. J. Hydrogen Energy. 39 (2014) 10927–10940. doi:10.1016/j.ijhydene.2014.05.021.

[32] M. Broda, A.M. Kierzkowska, D. Baudouin, Q. Imtiaz, C. Copéret, C.R. Müller, Sorbent-enhanced methane reforming over a Ni-Ca-based, bifunctional catalyst sorbent, ACS Catal. 2 (2012) 1635–1646. doi:10.1021/cs300247g.

[33] A. Kadkhodayan, A. Brenner, Temperature-programmed reduction and oxidation of metals supported on γ-alumina, J. Catal. 117 (1989) 311–321. doi:10.1016/0021-9517(89)90342-4.

[34] Y.H. Hu, Solid-solution catalysts for CO_2 reforming of methane, Catal. Today. 148 (2009) 206–211. doi:10.1016/j.cattod.2009.07.076.

[35] L. Sun, Y. Tan, Q. Zhang, H. Xie, F. Song, Y. Han, Effects of Y_2O_3-modification to Ni/γ-Al_2O_3 catalysts on autothermal reforming of methane with CO_2 to syngas, Int. J. Hydrogen Energy. 38 (2013) 1892–1900. doi:10.1016/j.ijhydene.2012.11.114.

[36] J.D.A. Bellido, E.M. Assaf, Effect of the Y_2O_3-ZrO_2 support composition on nickel catalyst evaluated in dry reforming of methane, Appl. Catal. A Gen. 352 (2009) 179–187. doi:10.1016/j.apcata.2008.10.002.

[37] H. Mori, C.J. Wen, J. Otomo, K. Eguchi, H. Takahashi, Investigation of the interaction between NiO and yttria-stabilized zirconia (YSZ) in the NiO/YSZ composite by temperature-programmed reduction technique, Appl. Catal. A Gen. 245 (2003) 79–85. doi:10.1016/S0926-860X(02)00634-8.

[38] H. Shang, K. Pan, L. Zhang, B. Zhang, X. Xiang, Enhanced activity of supported Ni catalysts promoted by Pt for rapid reduction of aromatic nitro compounds, Nanomaterials. 6 (2016) 103–117. doi:10.3390/nano6060103.

[39] X. Li, D. Li, H. Tian, L. Zeng, Z.J. Zhao, J. Gong, Dry reforming of methane over Ni/La_2O_3 nanorod catalysts with

stabilized Ni nanoparticles, Appl. Catal. B Environ. 202 (2017) 683–694. doi:10.1016/j.apcatb.2016.09.071.

[40] N.D. Charisiou, L. Tzounis, V. Sebastian, S.J. Hinder, M.A. Baker, K. Polychronopoulou, Investigating the correlation between deactivation and the carbon deposited on the surface of Ni/Al_2O_3 and Ni/La_2O_3-Al_2O_3 catalysts during the biogas reforming reaction, Appl. Surf. Sci. (2018) 0–1. doi:10.1016/j.apsusc.2018.05.177.

[41] O.H. Ojeda-Niño, F. Gracia, C. Daza, Role of Pr on Ni−Mg−Al Mixed Oxides Synthesized by Microwave- Assisted Self-Combustion for Dry Reforming of Methane, (2019). doi:10.1021/acs.iecr.9b00557.

[42] M.M. Barroso-Quiroga, A.E. Castro-Luna, Catalytic activity and effect of modifiers on Ni-based catalysts for the dry reforming of methane, Int. J. Hydrogen Energy. 35 (2010) 6052–6056. doi:10.1016/j.ijhydene.2009.12.073.

[43] L. Yao, M.E. Galvez, C. Hu, P. Da Costa, Synthesis Gas Production via Dry Reforming of Methane over Manganese Promoted Nickel / Cerium−Zirconium Oxide Catalyst, Ind. Eng. Chem. Res. 57 (2018) 16645–16656. doi:10.1021/acs.iecr.8b04183.

[44] L. Yao, M.E. Galvez, C. Hu, P. Da Costa, Mo-promoted Ni/Al_2O_3 catalyst for dry reforming of methane, Int. J. Hydrogen Energy. 42 (2017) 23500–23507. doi:10.1016/j.ijhydene.2017.03.208.

[45] H. Liu, P. Da Costa, H. Bel Hadjltaief, M. Benzina, M.E. Galvez, Mg-promotion of Ni natural clay-supported catalysts for dry reforming of methane, RSC Adv. 8 (2018) 19627–19634. doi:10.1039/C8RA02615G.

[46] H. Liu, K. Świrk, M.E. Galvez, P. Da Costa, Nickel supported modified ceria zirconia lanthanum/ praseodymium/yttrium oxides catalysts for syngas production through dry methane reforming, Mater. Sci. Forum. 941 (2018) 2214–2219. doi:10.4028/www.scientific.net/MSF.941.2214.

[47] A.I. Tsyganok, M. Inaba, T. Tsunoda, S. Hamakawa, K. Suzuki, T. Hayakawa, Dry reforming of methane over supported noble metals: A novel approach to preparing catalysts, Catal. Commun. 4 (2003) 493–498. doi:10.1016/S1566-7367(03)00130-4.

[48] B.K. Kim, G.H. Gwak, T. Okada, J.M. Oh, Effect of particle size and local disorder on specific surface area of layered double hydroxides upon calcination-reconstruction, J. Solid State Chem. 263 (2018) 60–64. doi:10.1016/j.jssc.2018.03.041.

[49] M. Mokhtar, A. Inayat, J. Ofili, W. Schwieger, Thermal decomposition, gas phase hydration and liquid phase reconstruction in the system Mg/Al hydrotalcite/mixed oxide: A comparative study, Appl. Clay Sci. 50 (2010) 176–181. doi:10.1016/j.clay.2010.07.019.

[50] I. Luisetto, S. Tuti, C. Battocchio, S. Lo Mastro, A. Sodo, Ni/CeO_2-Al_2O_3 catalysts for the dry reforming of methane: The effect of $CeAlO_3$ content and nickel crystallite size on catalytic activity and coke resistance, Appl. Catal. A Gen. 500 (2015) 12–22. doi:10.1016/j.apcata.2015.05.004.

[51] A. Sadezky, H. Muckenhuber, H. Grothe, R. Niessner, U. Pöschl, Raman microspectroscopy of soot and related carbonaceous materials: Spectral analysis and structural information, Carbon N. Y. 43 (2005) 1731–1742. doi:10.1016/j.carbon.2005.02.018.

[52] N.D. Charisiou, G. Siakavelas, K.N. Papageridis, A. Baklavaridis, L. Tzounis, K. Polychronopoulou, M.A. Goula,

Hydrogen production via the glycerol steam reforming reaction over nickel supported on alumina and lanthana-alumina catalysts, Int. J. Hydrogen Energy. 42 (2017) 13039–13060. doi:10.1016/j.ijhydene.2017.04.048.

[53] N.D. Charisiou, S.L. Douvartzides, G.I. Siakavelas, L. Tzounis, V. Sebastian, V.Stolojan, S.J. Hinder, M.A. Baker, K. Polychronopoulou, M.A. Goula, The relationship between reaction temperature and carbon deposition on nickel catalysts based on Al2O3, ZrO2 or SiO2 supports during the biogas dry reforming reaction, Catalysts, 9 (2019), pp. 676-69

[54] M. Khavarian, S.P. Chai, A.R. Mohamed, Direct use of as-synthesized multi-walled carbon nanotubes for carbon dioxide reforming of methane for producing synthesis gas, Chem. Eng. J. 257 (2014) 200–208. doi:10.1016/j.cej.2014.05.079.

[55] Z. Bao, Y. Lu, J. Han, Y. Li, F. Yu, Highly active and stable Ni-based bimodal pore catalyst for dry reforming of methane, Appl. Catal. A Gen. 491 (2015) 116–126. doi:10.1016/j.apcata.2014.12.005.

[56] J. Han, Y. Zhan, J. Street, F. To, F. Yu, Natural gas reforming of carbon dioxide for syngas over Ni–Ce–Al catalysts, Int. J. Hydrogen Energy. 42 (2017) 18364–18374. doi:10.1016/j.ijhydene.2017.04.131.

[57] Z.L. Zhang, X.E. Verykios, Carbon dioxide reforming of methane to synthesis gas over supported Ni catalysts, Catal. Today. 21 (1994) 589–595. doi:10.1016/0920-5861(94)80183-5.

[58] A.I. Tsyganok, T. Tsunoda, S. Hamakawa, K. Suzuki, K. Takehira, T. Hayakawa, Dry reforming of methane over catalysts derived from nickel-containing Mg-Al layered double hydroxides, J. Catal. 213 (2003) 191–203. doi:10.1016/S0021-9517(02)00047-7.